Nonlinear Charge Control for a Collinear Fixed Shape Three-Craft Equilibrium

Shuquan Wang and Hanspeter Schaub

Simulated Reprint from

Journal of Guidance, Navigation and Control

Volume 34, Number 2, Mar.–Apr., 2011, Pages 359–366

A publication of the
American Institute of Aeronautics and Astronautics, Inc.
1801 Alexander Bell Drive, Suite 500
Reston, VA 22091

JOURNAL OF GUIDANCE, NAVIGATION AND CONTROL
Vol. 34, No. 2, Mar.–Apr., 2011

Nonlinear Charge Control for a Collinear Fixed Shape Three-Craft Equilibrium

Shuquan Wang* and Hanspeter Schaub†

The collinear equilibrium three-craft formation charge feedback control problem is investigated. Given a charged equilibrium collinear configuration of spacecraft flying in deep space, a nonlinear charge feedback control algorithm is developed to stabilize the formation to the desired shape and size. The Coulomb forces are assumed to be acting along the line-of-sight directions between the bodies, and thus do not provide general vehicle position controllability. A study of the charged collinear three-craft formation shows that there exists an infinite number of equilibrium charge solutions for any collinear configuration. Given a real value of one spacecraft charge, the required equilibrium charges of the remaining two vehicles are solved analytically. A Lyapunov based nonlinear control algorithm is developed to stabilize the configuration to the equilibrium state using only the spacecraft charges as the control states. Real charge solutions are ensured by utilizing the one-dimensional solution null-space. Numerical simulations illustrate the new charge feedback control performance. In contrast to earlier efforts, collinear configurations are stabilized even in the presence of very large initial position errors.

I. Introduction

Electrostatic actuation methods in space environments have been investigated for many years. In 1966 Cover, Knauer and Maurer discuss in their U.S. patent application how active charge emission can be used to control the electrostatic potential of a reflecting membrane structure.[1] Here the outer membrane edge is held fixed by a solid support structure, while the absolute charge control is employed to electrostatically inflate the membrane itself. The absolute charge control is achieved using continuous emission of either positive (ion) or negatively (electrons) charged particles. With the space plasma environment encountered at geosynchronous orbit altitudes, they state that this charge control can be achieved using as little as Watt-levels of electrical power.

In the 1970's the SCATHA[2] and ATS-6 missions[3] studied the natural charging levels that can occur at geostationary altitudes, and found while flying through the Earth's shadow the hot plasma electrons can cause negative absolute charging reaching up to 10-20 kV. These missions also demonstrated that using active charge emission it is feasible to control the absolute potential of a space vehicle. The spacecraft potential was artificially increased to 15-20kV levels during sun-lit orbit conditions. Current geostationary spacecraft constructions does not typically employ active charge emission to avoid charging. Instead, the outer vehicle surface is constructed such that all components are conductively interconnected . This avoids the challenging differential charging and the associated electrostatic discharges, and allows the vehicle to homogeneously raise and lower its absolute potential. The later type of charging has a minimal impact on satellite operations.

By controlling the separation distances through electrostatic forces it is possible to achieve particular formation types such as Coulomb virtual tethers[4–6] or Coulomb virtual structures[7–10] as illustrated in Figure 1. The associated non-affine feedback control problem is very challenging to solve for a general cluster of spacecraft. However, there are three primary reasons that make the Coulomb Formation Flying (CFF) concept attractive in close proximity flying control. First, generating Coulomb forces is essentially propellant-less.[7] Second, CFF is very power-efficient, it requires only several Watts of electric power to operate, which is 3–5 orders of magnitude more power-efficient than Electric Propulsion (EP).[1] Third, because it is essentially propellant-less, it does not generate the caustic exhaust plumes as the ion thrusters do, which might cause some damage to the neighboring spacecraft. The CFF concept is thus appealing in long-term clustered-flying missions.

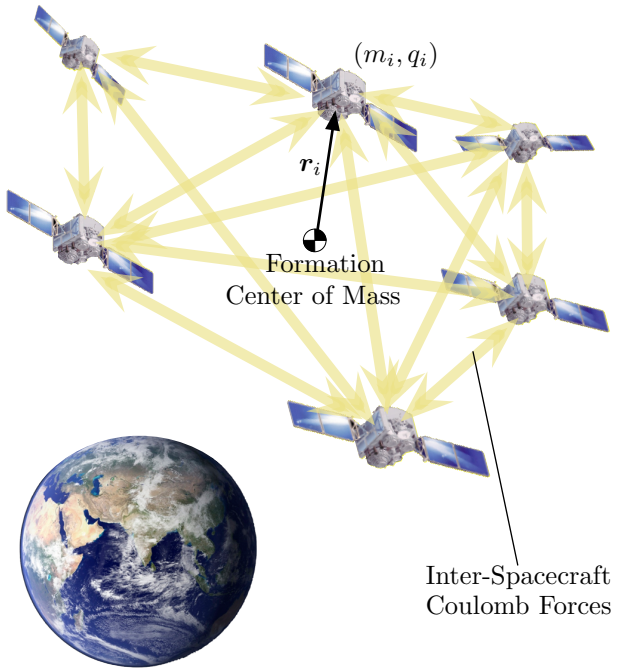

Figure 1: Illustration of a Charge Spacecraft Cluster in a Geosynchronous Orbit

On the other hand, CFF also encounters several challenges. First, in the vacuum the magnitude of the Coulomb force reduces quadratically as the separation distance increases. Thus the Coulomb force is proposed to control only tight formations with separation distances roughly within 100 meters. Second, the control development of the charged formation is very challenging. Unlike the inertial thrusters that can produce the control forces in any direction, the Coulomb force always lie essentially in the line-of-sight direction between two spacecraft. Thus the Coulomb forces form an under-actuated set of control forces to influence the general satellite relative positions and velocities. Another complication arises from the fact that the spacecraft charges, the control variables of a Coulomb control law, appear nonlinearly in the equations of motion. This leads to a complex non-affine control problem where mathematical complications such as imaginary or non-unique charge solutions must be accounted for.[8] Third, the plasma environment in space will partially shield the electrostatic force field that a neighboring charged satellite will experience, often re-

*Graduate Research Assistant, Aerospace Engineering Sciences Department, University of Colorado at Boulder, Boulder, CO. shuquan.wang@colorado.edu
†Associate Professor, AIAA Associate Fellow, AAS member, Aerospace Engineering Sciences Department, University of Colorado at Boulder, Boulder, CO.
Presented as Paper 06–3792 at the AIAA Guidance, Navigation and Control Conference, San Diego, CA, July 29–31, 1996.

ferred to as the Debye shielding effect.[11,12] The Debye shielding effect reduces the magnitude of the Coulomb force. The strength of the Debye shielding effect is measured by the Debye length, with a shorter Debye length implying stronger Debye shielding. Depending on the spacecraft potential, the Coulomb force magnitude can drop substantially when the separation distance is greater than the local Debye length.

The charge feedback control development of a general cluster of satellites remains an active area of research. Berrymann and Vasavada et al. study the equilibrium charges and positions for multi-satellite charged static virtual structures in References 8–10, 13. Natarajan et al. investigate the two-craft nadir Coulomb tether control problem in References 4–6, 14 where only linearized relative motion is considered. The European studies in References 15–17 and 18 look at hybrid techniques employing both electrostatic and inertial thrusting to control the relative motion of a swarm of spacecraft. Projection methods are used to map the set of required control forces onto the satellite line-of-sight vectors to determine a sub-set of control forces that can be achieved using active absolute electrostatic control, while the remaining control forces are created using inertial thrusting. Reference 19 studies the charge feedback control of a spinning two-craft formation at GEO. If both the inertial and relative position vectors of the two spacecraft are measurable, the control asymptotically stabilizes the separation distance to the expected distance. Otherwise, the boundaries of the error are developed in the situation that only the separation distance is fed back into the control algorithm.

Reference 20 studies the stability of a spinning two-craft Coulomb-tether where the system is assumed to be in deep space and not orbiting a planet. To date this spinning two-craft system is the only passively stable Coulomb spacecraft formation that has been found. Reference 21 studies the necessary relative equilibrium conditions for a spinning charged three-body system in deep space, and develops a simple linear feedback control to stabilize a collinear configuration. However, as discussed in Reference 21, the linear feedback control law has a very small area of convergence, and cannot handle large departure motions.

The focus of this paper is the development of a charge-only feedback control strategy to stabilize the 3-vehicle spacecraft motion relative to collinear equilibrium configurations subject to large departure motions. The spacecraft are assumed to operate in deep space, and the forces of differential gravity are ignored in this study. In Reference 19 the electrostatic shape control of a spinning two-craft system is discussed in both deep space and geostationary orbits. The deep space control strategy can be applied to the geostationary regime if the spin rate is sufficiently fast. For example, the differential gravity coupling is a function of the orbit period, 24 hours for geostationary orbits. If the spin rate of the Coulomb spacecraft cluster is much faster, on the order of hours or less, then the orbital motion can be treated as a small perturbation which is controlled through the shape feedback. Thus, while the current paper focuses on deep space applications without coupled orbital motion, the results are of interest for orbiting applications if the spin rate is large in comparison to the orbit rate. Strongly coupled spinning and orbiting motion where the Coulomb cluster spin rate is small is beyond the scope of this paper.

Prior work on the shape control of three charged vehicles requires hybrid control strategies,[17] or linear control solutions that are applicable only for very small departure motions.[21] References 22 and 23 are direct prior work upon which the new feedback control results of this paper are built. In particular, Reference 22 develops a nonlinear control for the one-dimensionally constrained three-craft Coulomb virtual structure. The general mapping from charge products to individual charges can yield imaginary charge solutions,[8] or charge solutions which require the vehicle to assume multiple potentials simultaneously.[10] In Reference 22 the control employs the null-space to determine charge solutions which are real, and not imaginary values. Reference 23 investigates the fixed triangular shape control of a three-craft Coulomb virtual structure in free space. In contrast to the collinear equilibrium configurations considered in this paper, for a general triangular shape there is no equilibrium charge solution. As a result the charge control will never settle to a constant value, but will continue to switch between real charges in the end state. Because not all three triangle side lengths can always be controlled through electrostatic forces, a stable two-side switched control strategy is developed based on the multiple Lyapunov function analysis tool developed by Branicky.[24] Here the control determines which two sides have the larges shape tracking error, and then uses the three spacecraft charges to negate these errors. Reference 22 develops analytical stability guarantees of the discontinuous control strategy. Careful feedback gain selections ensure that the tracking errors are Lyapunov-like across two discrete control time steps.

This paper investigates the collinear configuration control of a three-craft Coulomb virtual structure in free space. For a collinear configuration, there always exists a family of equilibrium solutions instead of a unique solution. This extra degree of freedom (DOF) can be utilized to develop an implementable real charge control solution. A switched Lyapunov-function-based nonlinear control is investigated to stabilize the separation distances to the desired distances corresponding to the expected fixed collinear configuration. Of interest is how the nonlinear control can stabilize the collinear configuration in the presence of system momentum uncertainties, as well as very large initialization errors.

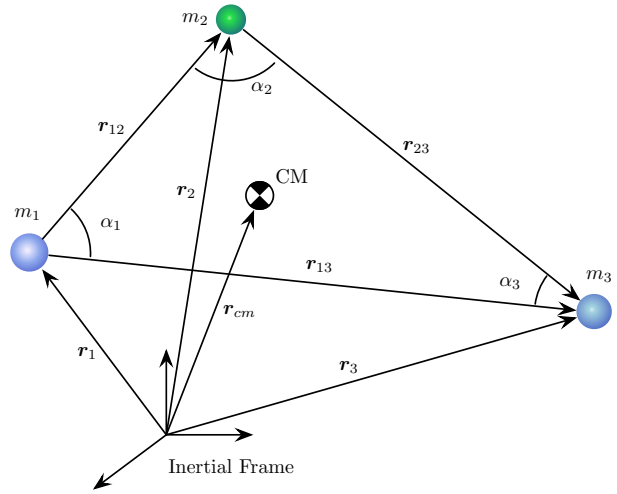

a) Geometry of the three-body system.

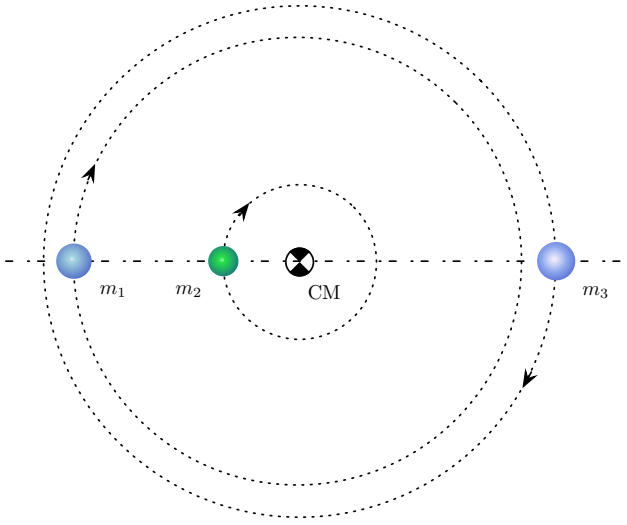

b) Collinear equilibrium illustration.

Figure 2: Charged three-Body system.

II. Equations Of Motion

This paper develops a control algorithm using only Coulomb forces to stabilize a free-flying three-craft system to a desired collinear configuration. Figure 2 shows the setup of the spinning

three-craft system. Figure 2(a) illustrates the basic geometry and notations. The parameters m_1–m_3 are the masses of the three spacecraft, $\boldsymbol{r}_1$–$\boldsymbol{r}_3$ are the three inertial position vectors of the spacecraft, $\boldsymbol{r}_{12}$–$\boldsymbol{r}_{13}$ are the relative position vectors between the spacecraft, and $\boldsymbol{r}_{cm}$ is the inertial position vector of the center of mass (CM). Note that if we let the center of the inertial frame be the CM of the 3-craft, then $\boldsymbol{r}_{cm} = \boldsymbol{0}$. The angle α_i is the angle between the two relative position vectors cornered at the i^{th} spacecraft. Figure 2(b) shows the scenario of the equilibrium/expected state. The collinear configuration system is spinning about the CM. Note that depending on the CM location, the spinning direction of m_2 may be reversed from the illustration in Figure 2(b).

For a sphere-like particle with charge q_1 immersed in a plasma environment with a Debye length λ_d, the potential ϕ at a distance r is expressed

$$\phi(r) = k_c \frac{q_1}{r} \mathrm{e}^{-r/\lambda_d}, \tag{1}$$

where $k_c = 8.99 \times 10^9$ Nm^2/C^2 is the Coulomb constant. This simple analytical solution for the potential about a point charge or sphere assumes that the electrostatic potential ϕ of the object is relatively small in comparison to the local plasma temperature.[11] For example, at geosynchronous orbit altitudes where the spacecraft fly through the Earth's plasma sheath, this potential threshold is about 1-10 kV. If the full Poisson-Vlaslov partial differential equations are solved instead of using a truncated version that yields the simple analytical result in Eq. (1), then large potentials can reduce the plasma charge shielding effect. This Coulomb force behavior is discussed in Reference 25 where the electrostatic forces to move an astroid in deep space are discussed. For example, effective Debye length $\hat{\lambda}_d$ can be multiple times the conventional Debye length. The partially shielded electrostatic potential $\phi(r)$ can be approximated up to the effective Debye length distance through[25]

$$\phi(r) = k_c \frac{q_1}{r} \mathrm{e}^{-r/\hat{\lambda}_d}, \tag{2}$$

The electrostatic force magnitude F_c that a second object with charge q_2 would experience is given by

$$F_c = \nabla_{\boldsymbol{r}} \phi \cdot q_2 = k_c \frac{q_1 q_2}{r^2} \mathrm{e}^{r/\hat{\lambda}_d} \left(1 + \frac{r}{\hat{\lambda}_d}\right) \tag{3}$$

In the following development we consider the case where the separation distances are smaller than the effective Debye length of the local plasma environment. While it is true that Debye lengths in the interplanetary medium at 1 AU from the sun can be 20-50 meters,[7] on the order of the craft separation distances, objects charged to high potentials (>1 kV) will experience effective Debye lengths many times larger.[25] Considering that such potential levels are proposed for Coulomb force actuation, it is a reasonable approximation to assume minimal Debye shielding effects for the current study. The electrostatic force in Eq. (3) must be considered a conservative lower bound on the achievable Coulomb actuation, while treating $\hat{\lambda}_d \to \infty$ provides the upper bound used in this paper. Because the separations distances considered are on the order of dozens of meters, and the effective Debye lengths are well into the 100's of meters, the resulting relative motion is dominated through the classical electrostatic force equations.

By the assumption that the three-craft system is flying in deep space (no differential gravity such as when orbiting a celestial body) with ignorable effective Debye lengths, the inertial equations of motion (EOMs) of the three spacecraft are given by

$$m_1 \ddot{\boldsymbol{r}}_1 = -k_c \frac{q_1 q_2}{r_{12}^2} \hat{\boldsymbol{e}}_{12} - k_c \frac{q_1 q_3}{r_{13}^2} \hat{\boldsymbol{e}}_{13} \tag{4a}$$

$$m_2 \ddot{\boldsymbol{r}}_2 = k_c \frac{q_1 q_2}{r_{12}^2} \hat{\boldsymbol{e}}_{12} - k_c \frac{q_2 q_3}{r_{23}^2} \hat{\boldsymbol{e}}_{23} \tag{4b}$$

$$m_3 \ddot{\boldsymbol{r}}_3 = k_c \frac{q_1 q_3}{r_{13}^2} \hat{\boldsymbol{e}}_{13} + k_c \frac{q_2 q_3}{r_{23}^2} \hat{\boldsymbol{e}}_{23} \tag{4c}$$

where q_i is the charge of the i^{th} spacecraft which can be actively controlled, $\hat{\boldsymbol{e}}_{ij}$ is the unit vector pointing from the i^{th} to the j^{th} spacecraft, and r_{ij} is the separation distance between the i^{th} and the j^{th} spacecraft. For the convenience of notation, a vector $\boldsymbol{\xi}$ is defined as a function of the charge products and the separation distances

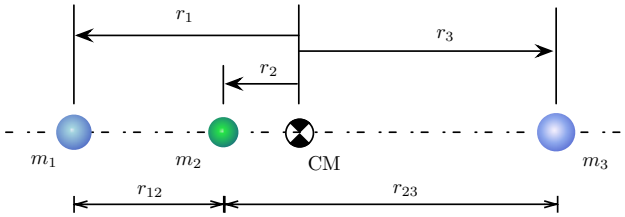

Figure 3: Geometries of the equilibrium state.

$$\boldsymbol{\xi} = (\xi_1,\ \xi_2,\ \xi_3)^T = \left(k_c \frac{q_1 q_2}{r_{12}^2},\ k_c \frac{q_2 q_3}{r_{23}^2},\ k_c \frac{q_1 q_3}{r_{13}^2}\right)^T \tag{5}$$

The collinear configuration is specified through the relationship of the separation distances

$$r_{13} = r_{12} + r_{23} \tag{6}$$

Using $\boldsymbol{r}_{ij} = \boldsymbol{r}_j - \boldsymbol{r}_i$the inertial EOMs in Eq. (4) are rewritten to yield the separation distance EOMs

$$\ddot{r}_{12} = \xi_1 \left(\frac{1}{m_1} + \frac{1}{m_2}\right) + \xi_2 \frac{1}{m_2} \cos\alpha_2 + \xi_3 \frac{1}{m_1} \cos\alpha_1 + g_1 \tag{7a}$$

$$\ddot{r}_{23} = \xi_1 \frac{1}{m_2} \cos\alpha_2 + \xi_2 \left(\frac{1}{m_2} + \frac{1}{m_3}\right) + \xi_3 \frac{1}{m_3} \cos\alpha_3 + g_2 \tag{7b}$$

$$\ddot{r}_{13} = \xi_1 \frac{1}{m_1} \cos\alpha_1 + \xi_2 \frac{1}{m_3} \cos\alpha_3 + \xi_3 \left(\frac{1}{m_1} + \frac{1}{m_3}\right) + g_3 \tag{7c}$$

Here the term g_i represents the following strongly nonlinear components

$$g_1 = \frac{1}{r_{12}} \|\dot{\boldsymbol{r}}_{12}\|^2 \left(1 - \cos^2 \angle(\boldsymbol{r}_{12},\ \dot{\boldsymbol{r}}_{12})\right) \tag{8a}$$

$$g_2 = \frac{1}{r_{23}} \|\dot{\boldsymbol{r}}_{23}\|^2 \left(1 - \cos^2 \angle(\boldsymbol{r}_{23},\ \dot{\boldsymbol{r}}_{23})\right) \tag{8b}$$

$$g_3 = \frac{1}{r_{13}} \|\dot{\boldsymbol{r}}_{13}\|^2 \left(1 - \cos^2 \angle(\boldsymbol{r}_{13},\ \dot{\boldsymbol{r}}_{13})\right) \tag{8c}$$

III. Collinear Equilibrium Charge Solution

The objective of the control development is to find an algorithm for the charges $[q_1, q_2, q_3]^T$ that makes the separation distances stabilize with respect to the desired distances $[r_{12}, r_{23}, r_{13}]^T \to [r_{12}^*, r_{23}^*, r_{13}^*]^T$, where the following requirement enforces the final configuration to be collinear

$$r_{13}^* = r_{12}^* + r_{23}^* \tag{9}$$

This section investigates the family of equilibrium charge solution for a given set of nominal collinear separation distances. Two questions must be answered: (1) Does the equilibrium charge solution exist? and (2) What is the solution space? Such insight is critical to the collinear feedback control development where the equilibrium charges can be employed in a feed-forward control component. This was not feasible in the prior three-vehicle triangular control in Reference 23 because no equilibrium charges existed for such nominal two-dimensional shapes.

For better physical understanding of the g_i, these nonlinear expressions are rewritten in terms of the angular momentum

$$\boldsymbol{g}^* = \begin{bmatrix} g_1^* \\ g_2^* \\ g_3^* \end{bmatrix} = \begin{bmatrix} r_{12}^* \frac{H^2}{(\Sigma m_i r_i^2)^2} \\ r_{23}^* \frac{H^2}{(\Sigma m_i r_i^2)^2} \\ r_{13}^* \frac{H^2}{(\Sigma m_i r_i^2)^2} \end{bmatrix} \tag{10}$$

where H is the magnitude of the angular momentum of the three-craft system $\boldsymbol{H} = \Sigma \boldsymbol{r}_i \times (m_i \dot{\boldsymbol{r}}_i)$. Because there are no external forces acting on the system due to the assumption on unperturbed deep space motion, the angular momentum is conserved, thus H is determined by the initial conditions. The scalar parameter r_i is the separation distance of the i^{th} spacecraft measured from the CM as shown in Figure 3. The relationship between r_i and r_{ij} is

$$\begin{cases} r_1 = \dfrac{m_2 + m_3(1+a)}{m_1+m_2+m_3} r_{12}^* \\ r_2 = r_1 - r_{12}^* \\ r_3 = r_1 - (1+a) r_{12}^* \end{cases} \tag{11}$$

where a is the ratio between the two separation distances $a = r_{23}^* : r_{12}^*$. Let us define the two charge ratio parameters as

$$\beta = \frac{q_2^*}{q_1^*}, \qquad \gamma = \frac{q_3^*}{q_1^*} \tag{12}$$

Thus, instead of solving the individual charges $[q_1^*, q_2^*, q_3^*]^T$ directly, the following derivation solves the parameters $[q_1^*, \beta, \gamma]$ corresponding to the individual charges. The separation distances' EOMs at the equilibrium state are derived from Eq. (7) to yield

$$\begin{aligned} \ddot{r}_{12}^* = &\frac{k_c q_1^{*2}}{r_{12}^{*2}} \left(\frac{1}{m_1} + \frac{1}{m_2} \right) \beta - \frac{k_c q_1^{*2}}{r_{12}^{*2}} \frac{1}{m_2} \frac{\beta\gamma}{a^2} \\ &+ \frac{k_c q_1^{*2}}{r_{12}^{*2}} \frac{1}{m_1} \frac{\gamma}{(1+a)^2} + g_1^* = 0 \end{aligned} \tag{13a}$$

$$\begin{aligned} \ddot{r}_{23}^* = &-\frac{k_c q_1^{*2}}{r_{12}^{*2}} \frac{1}{m_2} \beta + \frac{k_c q_1^{*2}}{r_{12}^{*2}} \left(\frac{1}{m_2} + \frac{1}{m_3} \right) \frac{\beta\gamma}{a^2} \\ &+ \frac{k_c q_1^{*2}}{r_{12}^{*2}} \frac{1}{m_3} \frac{\gamma}{(1+a)^2} + a g_1^* = 0 \end{aligned} \tag{13b}$$

$$\begin{aligned} \ddot{r}_{13}^* = &\frac{k_c q_1^{*2}}{r_{12}^{*2}} \frac{1}{m_1} \beta + \frac{k_c q_1^{*2}}{r_{12}^{*2}} \frac{1}{m_3} \frac{\beta\gamma}{a^2} \\ &+ \frac{k_c q_1^{*2}}{r_{12}^{*2}} \left(\frac{1}{m_1} + \frac{1}{m_3} \right) \frac{\gamma}{(1+a)^2} + (1+a) g_1^* = 0 \end{aligned} \tag{13c}$$

Next the solutions for $[q_1^*, \beta, \gamma]$ from Eq. (13) are found. Note that the three equations in Eq. (13) are linearly coupled, specifically adding up Eq. (13a) and Eq. (13b) yields Eq. (13c). Thus there are actually two independent equations for solving three parameters, yielding a one-dimensional null-space for the equilibrium charge solutions. Assuming that a value q_1^* is given, solving Eqs. (13a) and (13b) for γ yields the quadratic relationship

$$\begin{aligned} &\gamma^2 + \gamma \Big[(1+a)^2 \nu \big(m_1 m_2 + (1+a) m_1 m_3 \big) \Big] \\ &\qquad - (1+a)^2 a^2 \nu \big((1+a) m_1 m_3 + a m_2 m_3 \big) = 0 \end{aligned} \tag{14}$$

where ν is a function of q_1^*.

$$\nu = \frac{r_{12}^{*3} H^2}{k_c q_1^{*2} (\Sigma m_i r_i^2)^2 \Sigma m_i} \tag{15}$$

The other parameter β is given by

$$\beta = -\frac{\gamma}{(1+a)^2} - \nu \big(m_1 m_2 + (1+a) m_1 m_3 \big) \tag{16}$$

Thus, after solving γ from Eq. (14), the equilibrium charge solution is solved. To verify the existence of a real solutions to Eq. (14) requires the inequality

$$\begin{aligned} &f(\nu) = (1+a)^4 m_1^2 \big(m_2 + (1+a) m_3 \big)^2 \nu^2 + a^4 \\ &+ 2a^2 (1+a)^2 \big((1+a) m_1 m_3 + 2 a m_2 m_3 - m_1 m_2 \big) \nu \geq 0 \end{aligned} \tag{17}$$

where $f(\nu)$ is a quadratic function of ν. Note that ν is a function of q_1^* as shown in Eq. (15). For the inequality in Eq. (17), there are two cases need to be considered:

1. There are no real solutions or there are two identical solutions to $f(\nu) = 0$. In this case the inequality in Eq. (17) is always true. $m_1 \geq a m_2$ ensures this case.

2. There are two distinct solutions to $f(\nu) = 0$, corresponding to the situation $m_1 < a m_2$. In this case the requirement for ν is $\nu \geq \nu_2$ or $\nu \leq \nu_1$, where $\nu_{1,2}$ are the two real solutions to $f(\nu) = 0$ and $\nu_2 > \nu_1$.

   If $\nu_2 \leq 0$, any choice of q_1^* will automatically satisfy $\nu \geq \nu_2$, because $\nu > 0$ by definition. Otherwise $\nu_2 > 0$ and the requirement for q_1^* is

$$q_1^* \leq \sqrt{\frac{r^{*3} H^2}{k_c (\Sigma m_i r_i^2)^2 \Sigma m_i \nu_2}} \tag{18}$$

$$\text{or} \quad q_1^* \geq \sqrt{\frac{r^{*3} H^2}{k_c (\Sigma m_i r_i^2)^2 \Sigma m_i \nu_1}} \quad \text{if } \nu_1 > 0. \tag{19}$$

Concluding the above analysis of the existence of the equilibrium solutions, if $m_1 > a m_2$ or $\nu_2 \leq 0$, given any value of q_1^* there exists a pair of equilibrium solutions. Otherwise any value of q_1^* that satisfies the inequality in Eq. (18) results in a pair of equilibrium solutions.

IV. Lyapunov-Based Nonlinear Control Algorithm

Let us define the state vector $\boldsymbol{X}$ as

$$\boldsymbol{X} = (r_{12}, r_{23}, r_{13})^T \tag{20}$$

The control objective is for $\boldsymbol{X} \to \boldsymbol{X}^*$ where $\boldsymbol{X}^*$ represents the desired separation distances. The separation distance EOMs are rewritten as

$$\ddot{\boldsymbol{X}} = [B] \boldsymbol{\xi} + \boldsymbol{g} \tag{21}$$

where $[B]$ is the 3×3 matrix:

$$[B] = \begin{bmatrix} \frac{1}{m_1} + \frac{1}{m_2} & \frac{\cos\alpha_2}{m_2} & \frac{\cos\alpha_1}{m_1} \\ \frac{\cos\alpha_2}{m_2} & \frac{1}{m_2} + \frac{1}{m_3} & \frac{\cos\alpha_3}{m_3} \\ \frac{\cos\alpha_1}{m_1} & \frac{\cos\alpha_3}{m_3} & \frac{1}{m_1} + \frac{1}{m_3} \end{bmatrix} \tag{22}$$

Note that $\boldsymbol{\xi}$ is a function of the individual charges. The following development finds an implementable algorithm of $\boldsymbol{\xi}$ to stabilize the system. In the following context an implementable solution is a control that requires real, and not imaginary charge values.

Let us define the following Lyapunov candidate function

$$V = \frac{1}{2} \Delta \boldsymbol{X}^T [K] \Delta \boldsymbol{X} + \frac{1}{2} \Delta \dot{\boldsymbol{X}}^T \Delta \dot{\boldsymbol{X}} \tag{23}$$

to determine the 3-vehicle cluster shape tracking errors, where $[K]$ is a 3×3 positive definite matrix. Note that this V is a function of all three side errors. Thus, driving $V \to 0$ ensures that the three spacecraft converge to the desired spinning collinear shape. Taking the time derivative of V and utilizing the Eq. (21), yields

$$\begin{aligned} \dot{V} =& \Delta \dot{\boldsymbol{X}} ([K] \Delta \boldsymbol{X} + \Delta \ddot{\boldsymbol{X}}) \\ =& \Delta \dot{\boldsymbol{X}} \big([K] \Delta \boldsymbol{X} + [B] \boldsymbol{\xi} + \boldsymbol{g} \big) \end{aligned} \tag{24}$$

In order to utilize the equilibrium charge solution developed in the prior section, the control vector $\boldsymbol{\xi}$ is rewritten as

$$\boldsymbol{\xi} = \boldsymbol{\xi}^* + \delta \boldsymbol{\xi} \tag{25}$$

where $\boldsymbol{\xi}^*$ corresponds to the equilibrium charge solution. Forcing $\dot{V}$ to be the negative semi-definite form

$$\dot{V} = -\Delta \dot{\boldsymbol{X}}^T [P] \Delta \dot{\boldsymbol{X}} \tag{26}$$

yields the following equation

$$[B]\delta\boldsymbol{\xi} = -[P]\Delta\dot{\boldsymbol{X}} - [K]\Delta\boldsymbol{X} - [B]\boldsymbol{\xi}^* - \boldsymbol{g} \tag{27}$$

Solving $\delta\boldsymbol{\xi}$ from Eq. (27) yields a solution of $\boldsymbol{\xi}$ that would stabilize the system. One issue is that by the definition in Eq. (22) the matrix $[B]$ is not always invertible. The following theorem proves that the matrix $[B]$ is singular only at the collinear configurations.

Theorem 1 *Given a* 3×3 *matrix* $[B]$ *defined by Eq.* (22)*, with* $(\alpha_1, \alpha_2, \alpha_3)$ *being the inner angles of a triangle as shown in Figure 2(a), the matrix* $[B]$ *is singular if and only if* $\cos\alpha_1 \cos\alpha_2 \cos\alpha_3 = -1$.

One necessary and sufficient condition for a square matrix to be singular is that its determinant is zero. To prove the above theorem requires only that $\big|[B]\big| = 0$ if and only if (iff.) $\cos\alpha_1 \cos\alpha_2 \cos\alpha_3 = -1$. From the definition in Eq. (22), the determinant of $[B]$ is

$$\begin{aligned}\big|[B]\big| = &\left(\frac{1}{m_1}+\frac{1}{m_2}\right)\left(\frac{1}{m_2}+\frac{1}{m_3}\right)\left(\frac{1}{m_1}+\frac{1}{m_3}\right)\\ &+\frac{2\cos\alpha_1\cos\alpha_2\cos\alpha_3}{m_1m_2m_3} - \left(\frac{1}{m_1}+\frac{1}{m_2}\right)\frac{\cos^2\alpha_3}{m_3^2}\\ &-\left(\frac{1}{m_2}+\frac{1}{m_3}\right)\frac{\cos^2\alpha_1}{m_1^2} - \left(\frac{1}{m_1}+\frac{1}{m_3}\right)\frac{\cos^2\alpha_2}{m_2^2}\end{aligned} \tag{28}$$

Because $\cos^2\alpha_i \leq 1$, the following inequality is true.

$$\begin{aligned}\big|[B]\big| \geq &\left(\frac{1}{m_1}+\frac{1}{m_2}\right)\left(\frac{1}{m_2}+\frac{1}{m_3}\right)\left(\frac{1}{m_1}+\frac{1}{m_3}\right)\\ &+\frac{2\cos\alpha_1\cos\alpha_2\cos\alpha_3}{m_1m_2m_3} - \left(\frac{1}{m_1}+\frac{1}{m_2}\right)\frac{1}{m_3^2}\\ &-\left(\frac{1}{m_2}+\frac{1}{m_3}\right)\frac{1}{m_1^2} - \left(\frac{1}{m_1}+\frac{1}{m_3}\right)\frac{1}{m_2^2}\end{aligned} \tag{29}$$

Note that the equal relationship in Eq. (29) is true if and only if $\cos^2\alpha_i = 1,\ i = 1, 2, 3$. The right hand side of the inequality is simplified to

$$\big|[B]\big| \geq \frac{2 + 2\cos\alpha_1\cos\alpha_2\cos\alpha_3}{m_1m_2m_3} \tag{30}$$

From the inequality in Eq. (29), the determinant $\big|[B]\big| \geq 0$, $\big|[B]\big| = 0$ iff. $\cos\alpha_1\cos\alpha_2\cos\alpha_3 = -1$. □

Note that the necessary and sufficient condition for $\big|[B]\big| = 0$, $\cos\alpha_1\cos\alpha_2\cos\alpha_3 = -1$, represents all the collinear configurations, including the desired collinear configuration specified by $\boldsymbol{X}^*$.

Next the situations where $\big|[B]\big| = 0$ are discussed. At the equilibrium state where $\boldsymbol{X} = \boldsymbol{X}^*$, the state errors $\Delta\boldsymbol{X} = 0$ and $\Delta\dot{\boldsymbol{X}} = 0$. From the procedure of finding the equilibrium charge solution, at the equilibrium state $[B]\boldsymbol{\xi}^* + \boldsymbol{g} = 0$. Thus at the equilibrium state, the right hand side of Eq. (27) is zero. In this situation, any element in the null space of the singular matrix $[B]$ is the solution to Eq. (27), including the zero vector.

Another special case is the one-dimensional constraint motion that can result if the cluster has no angular momentum, and the spacecraft are lined up initially in a collinear configuration. This situation is discussed and studied earlier in Reference 22. In this case there are only two DOFs in the system and only two sides need to be controlled. Thus only two of the three equations in Eq. (27) are used in this scenario. Real charge control solutions are always obtainable in this special configuration.

Reference 23 discusses a switched control strategy where only the worst two shape-tracking errors are controlled at once. The three individual Lyapunov functions V_a, V_b and V_c track the shape errors of two sides of the triangular 3-vehicle cluster.

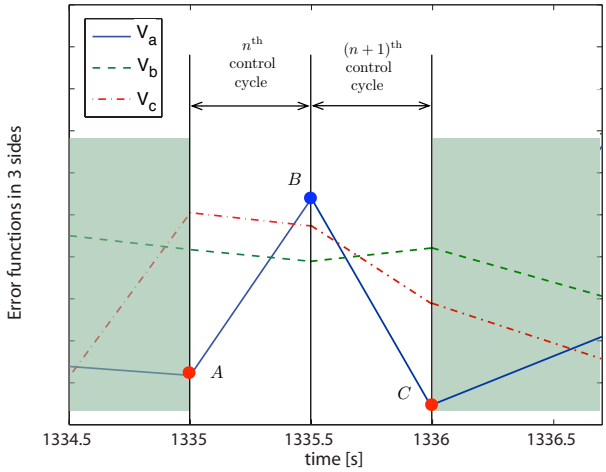

Figure 4: Illustration of the new two-side switching strategy with discrete control time steps.

$$V_a = \frac{1}{2}k(\Delta X_1^2 + \Delta X_3^2) + \frac{1}{2}(\Delta X_1^2 + \Delta X_3^2), \tag{31a}$$

$$V_b = \frac{1}{2}k(\Delta X_1^2 + \Delta X_2^2) + \frac{1}{2}(\Delta X_1^2 + \Delta X_2^2), \tag{31b}$$

$$V_c = \frac{1}{2}k(\Delta X_2^2 + \Delta X_3^2) + \frac{1}{2}(\Delta X_2^2 + \Delta X_3^2). \tag{31c}$$

Here the subscripts $(a,\ b,\ c)$ denote the errors of the two sides cornered at the (1st, 2nd, 3rd) spacecraft respectively. The final Lyapunov function candidate being activated is chosen to be the largest sub-Lyapunov function through

$$V_{\text{ctrl}} = \max\{V_a,\ V_b,\ V_c\}. \tag{32}$$

The overall Lyapunov function V_{ctrl} switches the control to the subset of triangle sides with the largest shape errors, and thus ensures that all shape errors are reduced to zero.

Overall stability is guaranteed for a discrete-time implementation by ensuring that the three Lyapunov functions $V_a - V_c$ are Lyapunov-like.[24] Here it is necessary that the controlled Lyapunov function does not increase every other control time step. The full stability discussion and implementation description is provided in Reference 23 and is too long to summarize in this paper. However, the primary concept for a function to be Lyapunov-like is graphically visualized in Figure 4. At time step A the control is attempting to reduce the value of the worst tracking error represented through V_c. At time step B both V_b and V_c are reduced, but the error V_a has now become the largest. Thus, between time steps B and C the control reduces the shape error measure V_a. For V_a to be Lyapunov-like, it is necessary that $V_a(t_C) \leq V_a(t_A)$. Otherwise, it is possible for the overall error to slowly grow larger during the switching even while the worst shape errors are being reduced during a particular control interval. To guarantee that $V_a(t_C) \leq V_a(t_A)$ during the switching Reference 23 outlines a feedback gain modification technique that ensures this requirement.

Thus, during periods where the $[B]$ matrix is singular, or periods where the $\delta\boldsymbol{\xi}$ solution from Eq. (27) does not translate to real individual charges q_i, the switching two-side control from Reference 23 is employed again for the collinear three-spacecraft control. The two-side control will always yield real charge solutions, and reduce the worst shape tracking errors.[22,23] However, note that in contrast to non-equilibrium triangle shape control where there are no constant and real equilibrium charges to use in a feedforward control component, for the present collinear three-spacecraft control the earlier study in Reference 21 discusses that there exists a neighborhood about the equilibrium where all three sides are simultaneously controllable. Thus, as a consequence, as the three

sides begin to approach the desired collinear configuration, the presented control strategy is guaranteed to enter a neighborhood where all three sides can be controlled at once, and the shape asymptotically converges to the desired values while the charges approach the constant equilibrium charge solutions.

V. Numerical Simulations

This section illustrates the charge feedback control performance through the use of numerical simulations. The equations of motion in Eq. (4) are integrated using a variable time step 4th order Runge-Kutta integrator. The initial conditions are as following:

$$\boldsymbol{r}_1 = [-4, 1, 0]^T \text{ m} \tag{33a}$$

$$\boldsymbol{r}_2 = [25, 0, 0]^T \text{ m} \tag{33b}$$

$$\boldsymbol{r}_3 = [40, 0, 0]^T \text{ m} \tag{33c}$$

$$\dot{\boldsymbol{r}}_1 = [0, 0.001, 0.0001]^T \text{ m/s} \tag{33d}$$

$$\dot{\boldsymbol{r}}_2 = [0, 0, 0]^T \text{ m/s} \tag{33e}$$

$$\dot{\boldsymbol{r}}_3 = [0, 0.001, 0]^T \text{ m/s} \tag{33f}$$

The masses of the spacecraft are $m_1 = m_2 = m_3 = 50$kg. The controller coefficients are $[P] = 0.00015 I_{3\times3}$ s^{-1}, $[K] = 10^{-8} I_{3\times3}$ s^{-2}, where $I_{3\times3}$ is the 3×3 identity matrix. The nominal separation distances for the desired collinear configuration are $\boldsymbol{X}^* = [20, 20, 40]^T$m. Two scenarios are simulated. The first simulation illustrates the charge feedback control performance if the spacecraft are relatively close to their desired configuration. The second simulation illustrates a setup where the shape errors are very large. In all simulations a dead-band is implemented on the shape control. The threshold for turning off the feedback part is $V = 10^{-11}\text{m}^2/\text{s}^2$. This creates a more realistic simulation scenario, but will prevent the shape tracking errors from perfectly converging to zero.

A. Case 1 with Nominal Shape Errors

Figure 5 simulates a scenario where the multi-meter level shape errors are present. The relative position and velocity vectors of the spacecraft are assumed to be known. Figure 5(a) shows the resulting trajectories as seen from the inertial frame. The boxes represent the final locations of the three spacecraft, illustrating that they have converged to a collinear configuration.

Figure 5(b) shows the time histories of the separation distances. The nominal separation distance levels of 20 and 40 meters are also drawn for reference. The shape tracking errors smoothly approach the desired values. Figure 5(c) shows the separation distance errors in log scale to better illustrate the final control performance when the tracking errors become small. The reason that the shape tracking errors do not asymptotically converge to zero is because of the tracking error dead-band. The feedback component of the charge control is turned off if $V < 10^{-11}\text{m}^2/\text{s}^2$. Figure 5(c) shows that the distance error levels settle down to centimeter level. Compared to the linear controller used in Reference 21 where the initial separation distance errors are only 1-5%, the new nonlinear controller allows much larger shape errors to be controlled such as the 50% errors shown in this simulation.

Figure 5(d) shows the charge histories. There are three situations of the control: 3-side feedback control when $[B]$ is invertible; 2-side switched feedback control when $[B]$ is not invertible; only feedforward control when $V < 10^{-11}\text{m}^2/\text{s}^2$. Figure 5(d) illustrates time control regions where either of these cases occur. When the tracking errors fall below the dead-band threshold, the spacecraft charges are held constant. However, because these collinear equilibrium configurations are unstable, even small residual shape errors will grow large, thus triggering the charge feedback control to be engaged again. Further, note that charge changes in the desired charge states as the control switches between candidate Lyapunov functions. The control simulation updates the charges every few seconds. This is practical in that the electrostatic charge response of a spacecraft can go from zero to maximum charging within a few milli-seconds. For the control purposes in this study with maneuver periods of several hours, the charge changes can be considered essentially instantaneous.

B. Case 2 with Large Configurations Shape Errors

This simulation case is an example that uses very large to illustrate that the control works globally. In this challenging scenario the controller needs to reverse the locations of two spacecraft. The simulation conditions are the same as with the previous simulation except that the locations of the three spacecraft are set to:

$$\boldsymbol{R}_1 = [-4, 1, 0]^T \text{ m} \tag{34}$$

$$\boldsymbol{R}_2 = [40, 0, 0]^T \text{ m} \tag{35}$$

$$\boldsymbol{R}_3 = [25, 0, 0]^T \text{ m} \tag{36}$$

The equilibrium charges are assumed to be accurately computed in this setup. With this set of initial conditions, SC-3 is roughly allocated in the center of the nearly collinear configuration. While the expected collinear configuration requires SC-2 be the center of the configuration, the controller needs to reverse the relative positions of SC-2 and SC-3.

The simulation results are shown in Figure 6. The relative trajectories in Figure 6(a) are more complex than earlier due to the required reshuffling of the spacecraft positions. However, the final positions marked by the three boxes show that the three spacecraft are aligned again in a near-collinear configuration.

Figure 6(b) shows that L_{23} and L_{13} stabilize to their expected values after around 10 hours, L_{12} grows up to 60m, then stabilizes after around 40 hours. The distance errors in Figure 6(c) show that the error of L_{12} stabilizes to centimeter level, while the errors in L_{23} and L_{13} are at much lower level. While the earlier simulations considered initial separation distance errors on the order of 50%, this case illustrates initial errors of more than 100% still yield a stable long-term response.

Figure 6(d) shows that there is a spike of the control charges goes up to 80μC. Practically this charge level is very difficult to achieve using current technology. In CFF the charge levels are typically held around 1–10 μC which corresponds to a few dozen kilo-Volts depending on the spacecraft capacitance. The presented charge solutions are not unique to the non-uniqueness of the equilibrium charges. Future research could investigate alternate solution methods to reduce the absolute charge requirements. Further, the current control does not consider charge saturation issues. However, this dramatic collinear reconfiguration simulation illustrates well the global nature in which the charge feedback control can stabilize the spinning spacecraft cluster to desired collinear configurations.

VI. Conclusion

This paper develops a Lyapunov-based globally stable control algorithm to make a three-craft Coulomb formation stable about a desired equilibrium collinear configuration. For any collinear configuration there exists a family of charge solutions that satisfy the equilibrium conditions. The equilibrium charge solution is utilized as the feedforward part of the control to allow asymptotic convergence in contrast to the triangular shape control case. The two-side switched control strategy is engaged when the simultaneous three-side is not implementable with real charges. Numerical simulations illustrate the effectiveness of the switched control strategy to stabilize even very large configuration shape errors.

References

[1] J. H. Cover, W. Knauer, and H. A. Maurer, "Lightweight Reflecting Structures Utilizing Electrostatic Inflation," US Patent 3,546,706, October 1966.

[2] E. G. Mullen, M. S. Gussenhoven, D. A. Hardy, T. A. Aggson, and B. G. Ledley, "SCATHA Survey of High-Voltage Spacecraft Charging in Sunlight," *Journal of Geophysical Research*, Vol. 91, No. A2, 1986, pp. 1474–1490, doi:10.1029/JA091iA02p01474.

[3] E. C. Whipple and R. C. Olsen, "Importance of differential charging for controlling both natural and induced vehicle potentials on ATS-5 and ATS-6," *Proceedings of the 3rd Spacecraft Charging Technology Conference*, Nov. 12–14 1980, p. 887. NASA Conference Publication 2182.

[4] A. Natarajan and H. Schaub, "Hybrid Control of Orbit Normal and Along-Track Two-Craft Coulomb Tethers," *Aerospace Science and Technology*, Vol. 13, June–July 2009, pp. 183–191.

[5] A. Natarajan and H. Schaub, "Linear Dynamics and Stability Analysis of a Coulomb Tether Formation," *AIAA Journal of Guidance, Control, and Dynamics*, Vol. 29, July–Aug. 2006, pp. 831–839.

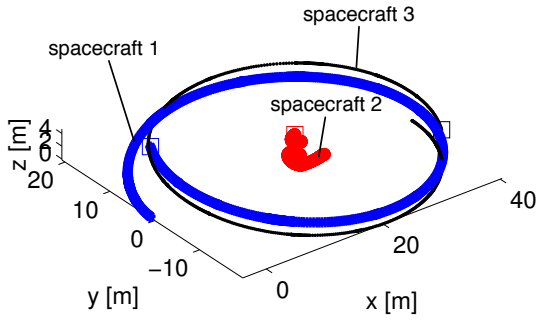

a) Inertial trajectories of the 3 craft.

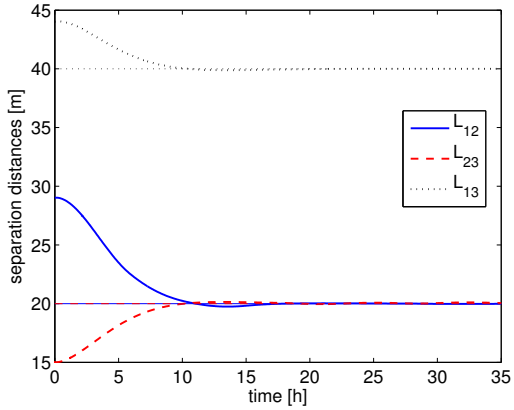

b) Separation distances.

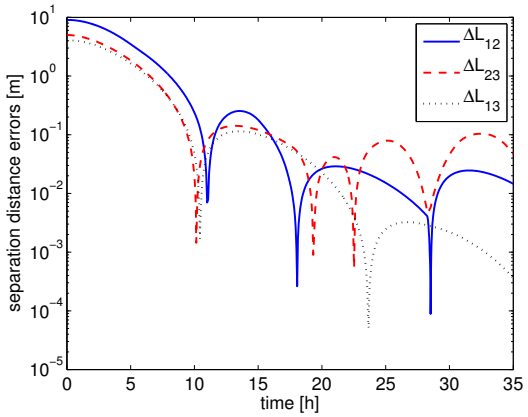

c) Magnitudes of the separation distance errors.

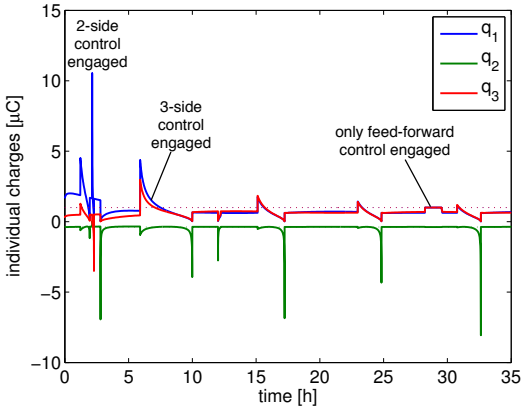

d) Individual charges.

Figure 5: Simulation results with the exact knowledge of the angular momentum.

[6] A. Natarajan and H. Schaub, "Orbit-Nadir Aligned Coulomb Tether Reconfiguration Analysis," *Journal of the Astronautical Sciences*, Vol. 56, Oct. – Dec. 2008, pp. 573–592.

[7] L. B. King, G. G. Parker, S. Deshmukh, and J.-H. Chong, "Spacecraft Formation-Flying using Inter-Vehicle Coulomb Forces," tech. rep., NASA/NIAC, January 2002. http://www.niac.usra.edu. (visited on December 1, 2010)

[8] J. Berryman and H. Schaub, "Analytical Charge Analysis for 2- and 3-Craft Coulomb Formations," *AIAA Journal of Guidance, Control, and Dynamics*, Vol. 30, Nov.–Dec. 2007, pp. 1701–1710.

[9] H. Schaub, C. Hall, and J. Berryman, "Necessary Conditions for Circularly-Restricted Static Coulomb Formations," *Journal of the Astronautical Sciences*, Vol. 54, July-Dec. 2006, pp. 525–541.

[10] H. Vasavada and H. Schaub, "Analytic Solutions for Equal Mass Four-Craft Static Coulomb Formation," *Journal of the Astronautical Sciences*, Vol. 56, Jan. – March 2008, pp. 7–40.

[11] D. R. Nicholson, *Introduction to Plasma Theory*. Malabar, FL: Krieger, 1992. pp. 1–3.

[12] J. A. Bittencourt, *Fundamentals Of Plasma Physics*. Springer-Verlag New York, Inc., 175 Fifth Avenue, New York, NY, 2004. pp. 273–278.

[13] J. Berryman and H. Schaub, "Static Equilibrium Configurations in GEO Coulomb Spacecraft Formations," *Advances in Astronautical Sciences*, Vol. 120, American Astronautical Society, 2005, pp. 51–68. Paper No. AAS 05–104.

[14] A. Natarajan, H. Schaub, and G. G. Parker, "Reconfiguration of a Nadir-Pointing 2-Craft Coulomb Tether," *Journal of British Interplanetary Society*, Vol. 60, June 2007, pp. 209–218.

[15] V. J. Lappas, C. Saaj, D. J. Richie, M. A. Peck, B. Streetman, and H. Schaub, "Spacecraft Formation Flying and Reconfiguration with Electrostatic Forces," *Advances in Astronautical Sciences*, Vol. 127, American Astronautical Society, 2007, pp. 217–226. Paper AAS 07–113.

[16] C. Saaj, V. J. Lappas, H. Schaub, and D. Izzo, "Hybrid propulsion system for formation flying using electrostatic forces," *Aerospace Science and Technology*, Vol. 14, No. 5, 2010, pp. 348 – 355, DOI: 10.1016/j.ast.2010.02.009.

[17] L. Pettazzi, D. Izzo, and S. Theil, "Swarm Navigation and Reconfiguration using Electrostatic Forces," *7th International Conference on Dynamics and Control of Systems and Structures in Space*, Greenwich, London, England, July 2006, pp. 257–267.

[18] L. Pettazzi, H. Krüger, S. Theil, and D. Izzo, "Electrostatic Forces for Satellite Swarm Navigation and Reconfiguration," *2^{nd} ACT Workshop on Innovative Concepts*, ESTEC, 2008.

[19] S. Wang and H. Schaub, "Nonlinear Coulomb Feedback Control of a Spinning Two Spacecraft Virtual Structure," *Advances in Astronautical Sciences*, Vol. 135, American Astronautical Society, 2009, pp. 1477–1496. Paper AAS 09–393.

[20] H. Schaub and I. I. Hussein, "Stability and Reconfiguration Analysis of a Circulary Spinning 2-Craft Coulomb Tether," *IEEE Aerospace Conference*, Big Sky, MT, March 3–10 2007. Paper No. IEEEAC-1361.

[21] I. I. Hussein and H. Schaub, "Stability and Control of Relative Equilibria for the Three-Spacecraft Coulomb Tether Problem," *Acta Astronautica*, Vol. 65, No. 5–6, 2009, pp. 738–754, doi:10.1016/j.actaastro.2009.03.035.

[22] S. Wang and H. Schaub, "1-D Constrained Coulomb Structure Stabilization With Charge Saturation," *Advances in Astronautical Sciences*, Vol. 129, Mackinac Island, MI, American Astronautical Society, 2007, pp. 257–274. Paper AAS 07–267.

[23] S. Wang and H. Schaub, "Switched Lyapunov Function Based Coulomb Control of a Triangular 3-Vehicle Cluster," *Advances in Astronautical Sciences*, Vol. 135, American Astronautical Society, 2009, pp. 1477–1496. Paper AAS 09–391.

[24] M. Branicky, "Multiple Lyapunov functions and other analysis tools for switchedand hybrid systems," *Automatic Control, IEEE Transactions on*, Vol. 43, No. 4, 1998, pp. 475–482.

[25] N. Murdoch, D. Izzo, C. Bombardelli, I. Carnelli, A. Hilgers, and D. Rodgers, "The Electrostatic Tractor for Asteroid Deflection," *58th International Astronautical Congress*, 2008. Paper IAC-08-A3.I.5.

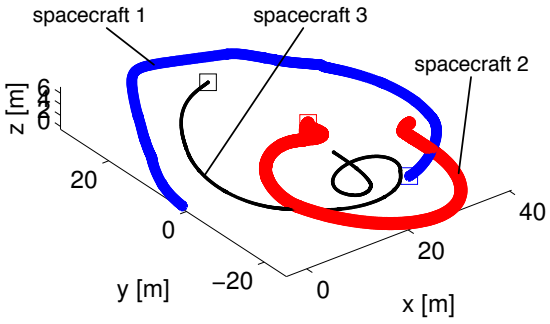

a) Inertial trajectories of the 3 craft.

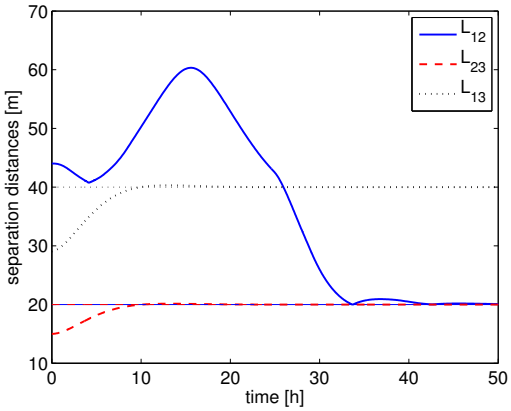

b) Separation distances.

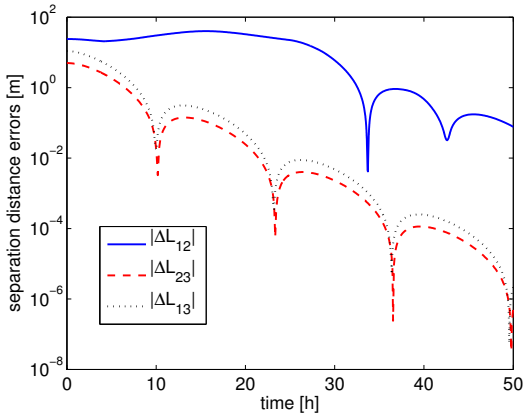

c) Magnitudes of the separation distance errors.

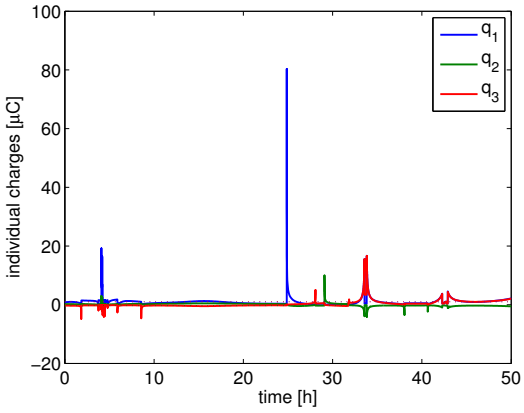

d) Individual charges.

Figure 6: Simulation results without the exact knowledge of the angular momentum.